

An Investigation of the Properties of BCP Niobium for Superconducting RF Cavities

Anatolii Polyanskii¹, Pierre Bauer², Peter J. Lee¹, Cristian Boffo²,
Leo Bellantoni², Helen Edwards², Alex Gurevich¹, Matt Jewell¹,
David Larbalestier¹, G.K. Perkins³, Alex Squitieri¹

1 Applied Superconductivity Center- University of Wisconsin at Madison

2 Fermilab

3 Blackett Laboratory, Imperial College of Science and Technology and Medicine

Abstract. FNAL and the Applied Superconductivity Center at the University of Wisconsin-Madison have started a collaboration to perform basic research into superconducting RF materials. Our primary thrust is to gain a better understanding of the effect of grain boundaries on the RF surface resistance, using a combination of magneto-optics, surface analysis with electron microscopy and XPS and transport measurements. Preliminary magneto-optical measurements on mm-size grain samples revealed preferential flux penetration through the grain-boundaries consistent with depressed superconductivity in certain grain boundaries. New experiments are planned that will measure the inter-grain critical current. We report on the progress of this collaboration.

INTRODUCTION

Two types of 3.9 GHz superconducting RF cavities are under development at FNAL for use in the upgraded A0 photo-injector facility. A TM110 mode cavity will provide streak capability for bunch slice diagnostics, and a TM010 mode cavity will provide linearization of the accelerating gradient before compression for better emittance^[1]. In this context Fermilab has been steadily developing its SRF cavity expertise, infrastructure and technology base. Recently Fermilab and the Applied Superconductivity Center (ASC) at the University of Wisconsin (UW) have joined forces to investigate the properties of the high purity niobium used in the cavity fabrication. Besides microscopy and chemical analysis, the focus of the material investigation is on so-called “superconducting” methods such as magnetization, specific heat and magneto-optics.

Magnetization and magneto-optical measurements probe the bulk superconducting properties of the material. These methods also allow us to measure flux penetration. This is particularly important since it is believed that the penetration of small numbers of flux lines into the cavity surface during RF operation is almost certainly leading to breakdown of the superconducting state. The understanding of DC flux penetration is the first step towards the understanding flux penetration in RF fields. Fermilab provided samples to the UW for testing. The samples were selected to represent the material and surface condition found on the side of the cavities exposed to RF fields, such as samples representative of the weld region as well as the rest of the cavity surface. The following discusses the results of the magnetic characterization of these samples with electron microscopy, magnetization and magneto-optics.

¹ pbauer@fnal.gov, lee@engr.wisc.edu

DESCRIPTION OF THE SAMPLES

Two sets of samples made from Wah Chang high purity niobium were provided by Fermilab to UW for experimental analysis. These samples were selected to represent the material and surface condition found on the side of the cavities exposed to RF fields. The first set was cut from electron beam welds, such as those performed to weld deep-drawn half-cells into multi-cell cavities. The weld samples were fabricated from 1.6 mm thick, RRR 350 material. The weld samples were characterized by large grains obtained by the melting of the material during welding. The weld samples were also characterized by deep grain-boundary grooving. The second set of samples consisted of wrought material (2.2 mm thick, RRR 450), whose linear intercept grain size was ~50 microns (~55 microns after the 800°C heat treatment). Both sets of samples were cut by wire EDM into different shapes for the various measurements and treated in the same way as the inner cavity surfaces, including various etchings and heat treatments. The only (but notable!) exception is that the regular sheet material was not mechanically deformed, as the cavity material is during deep drawing. The preparation steps comprised of two BCP (1:1:2) etching stages and a high temperature heat treatment. The first etching step removed ~100 microns and with it the mechanical defects introduced into the surface by deep-drawing (or wire erosion cutting in this case). The heat treatment (800°C, 5 hrs) served to outgas the hydrogen introduced into the material by the etching and to anneal the previously work-hardened material. The second, light etching step served to remove the surface contamination introduced by the heat treatment. Rinsing with ultra-pure water and drying with filtered nitrogen, was always performed in a class 1000 clean-room. The samples were transported either in high purity water or in polyethylene tubes containing dry nitrogen as buffer gas. The exposure of the samples, especially following the heat treatment was thus kept to the minimum (extraction of samples from furnace or acid bath).

Table 1 lists the major preparation steps for the different samples provided for this study. The third type of sample listed in this table consisted of a few samples from the regular sheet material, which underwent an additional 1250°C / 24 hrs heat treatment (and subsequent ~50 micron BCP etching) to grow large grains for further study of the flux penetration into the large grain samples. This special heat treatment was performed by A.-M. Valente of TJNAF. Fig. 1 shows micrographs obtained with light and electron microscopy of the two basic sets of samples studied. On the left a 3D optical image of the weld sample is shown. On the right a 3D-SEM of regular type sample is shown. The grains in the weld sample are mm-sized, while the grains in the regular sample are ~50 microns. The surface smoothness also appears to be very different. A particular feature of the weld sample is the depth of the grain boundaries. Fig. 2 shows an example of a depth profile through two grain-boundaries, obtained with the MEX software². The depth of the grain boundary measured in this way is ~1 micron. This value has to be compared to the London penetration depth in niobium, ~40 nm, that is the thickness of the layer in which the RF shielding super-current is flowing.

TABLE 1. High purity Niobium samples for the UW-FNAL material investigation.						
Sample	Comment	#	Clean	Etch 1	Heat	Etch 2
BCP1_W_HT1_RRR	RRR type, from e-beam weld, 1.6 mm thickness, RRR~350	3	2x(US-M90 + UPW, rinse until 12MΩ) dried in lam N2	BCP 1:1:2 at ~15-18 C 100 min, rinse in UPW	800 C 5 hrs 10 ⁶ Torr	BCP 1:1:2 at 17.5 C 20 min, rinse in UPW
BCP2_S_HT1_RRR	RRR type, from regular sheet, 2.2 mm thickness, RRR~450	10	2x(US-M90 + UPW rinse until >10MΩ) dried in lam N2	BCP 1:1:2 at ~15 C 80 min, rinse in UPW	800 C 5 hrs 10 ⁶ Torr plateau: 24 hrs 400 C	BCP 1:1:2 at ~15C 20 min rinse in UPW
BCP2_S_HT1_MO	magneto-optics	5				
BCP2_S_HT1_MAG	magnetization	3				
BCP2_S_HT1_BC	bi-crystal	4				
BCP2_S_HT1_M	microscopy	3	— —	— —	— —	— —
BCP2_S_HT2_RRR	taken from above	1	same as above + heat treatment (1250C, 24 hrs) at TJNAF (AM Valente) and etch (50 min, BCP1:1:2) to grow large grains			
BCP2_S_HT2_MO		1				

² Example of profilometric measurement using MEX, demo provided by A. Groeber / Alicona Imaging GmbH.

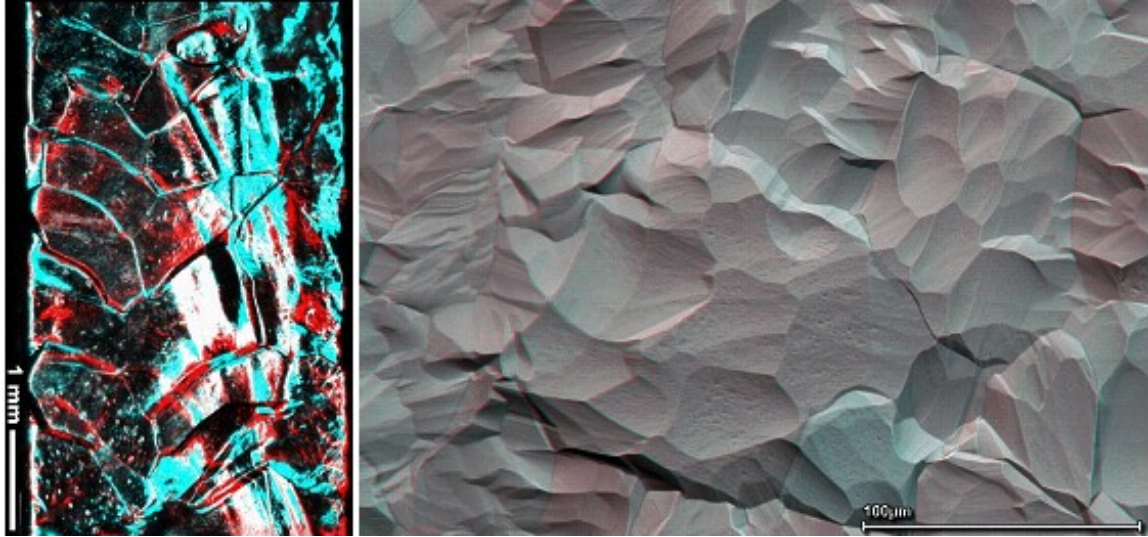


FIGURE 1. Left: 3D-light microscopy of weld sample. Right: 3D-SEM of regular type sample.

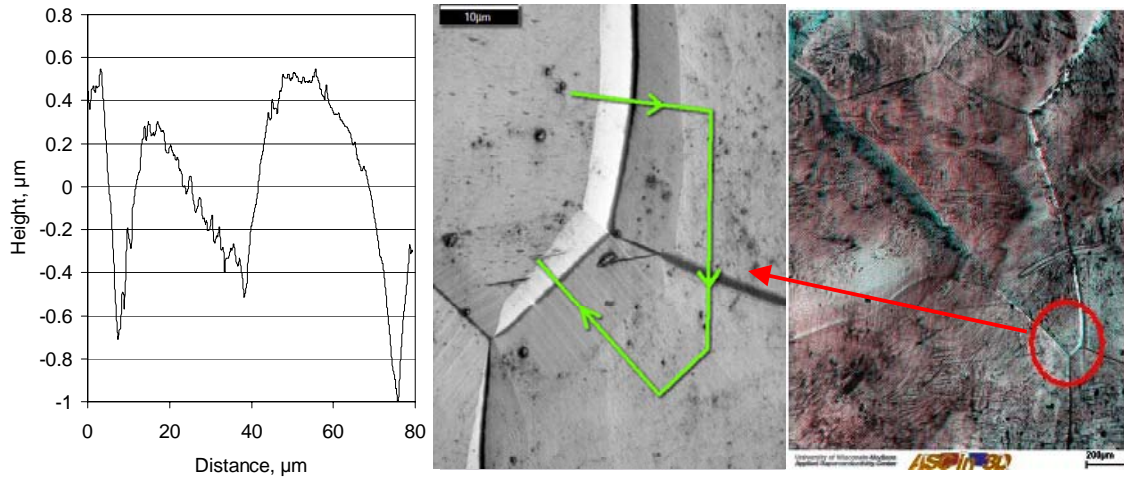


FIGURE 2. Left: Grain boundary profile in weld sample obtained with MEX. Right: 3D SEM zoom into weld sample.

The topological features found in the Fermilab samples is for the most part consistent with the results of similar surface characterization campaigns reported in literature, such as for instance in [2].

MAGNETIZATION MEASUREMENTS

The measurement of DC magnetization serves the purpose of providing a quantitative measure of the average magnetic and superconducting properties of the bulk-material. Such magnetization measurements were performed at Fermilab by flux integration. The Fermilab DC magnetization measurement is described further in [3]. The samples tested were obtained by deforming the sheet material into long, hollow cylinders. This step introduced strong cold working into the material, not unlike in the deep-drawing stage of the fabrication of the cavities. The resulting magnetization curve, shown in Fig. 3, clearly reflects the expected type II behavior, with flux penetrating into the bulk at $H \approx H_{c1}$. Pinning of vortices leads to an irreversible magnetization component and hysteresis. The pinning is reduced following the heat treatment (5 hrs, 800°C). Interestingly, the higher critical field H_{c2} is not affected by the heat treatment. This indicates that the mean free path in the bulk was not affected by the heat treatment (the fact that the RRR also

remained unchanged further corroborates this fact). This indicates that the pinning actually occurs in the surface. The H_{c2} values found (~ 287 mT) are slightly higher than theoretically expected, further indicating enhanced defect- and/or contamination density in the surface. The small bump of the magnetization curve just below H_{c2} , especially in the before annealing case, is thought to be a related effect.

Using the data shown in Fig. 3, the lower and upper critical fields were read from the curves. The critical fields at 4.2 K are $\mu_0 H_{c1} \sim 140$ mT, $\mu_0 H_{c2} \sim 285$ mT. The 4.2 K values were used to calibrate a standard function describing the temperature dependence of the critical fields. Using this function (see Fig. 3, right graph) the critical fields at 6 K become $\mu_0 H_{c1} \sim 88$ mT, $\mu_0 H_{c2} \sim 177$ mT. At 7 K they are $\mu_0 H_{c1} \sim 59$ mT, $\mu_0 H_{c2} \sim 118$ mT. The important parameters derived from the magnetization measurements helped us interpret the magneto-optical measurements. Also shown in Fig. 3 is the MO penetration field, i.e. the field at which flux first penetrates into the samples. The magneto-optical measurements will be discussed next.

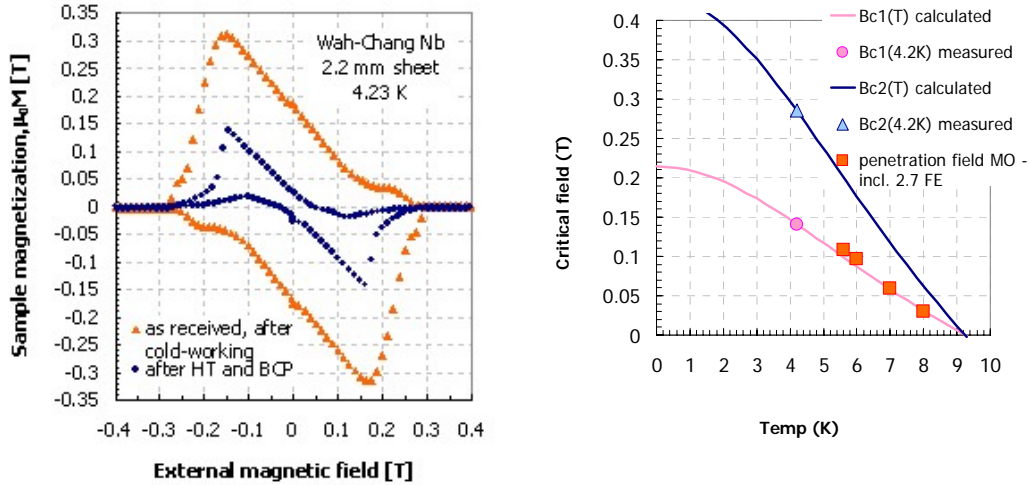


FIGURE 3. Left: Magnetization measured on samples of niobium for the Fermilab SRF cavities before and after annealing. Right: Calculated extrapolation of critical magnetic fields to higher temperatures. Also shown are the fields at which magnetic flux first penetrates the magneto-optics samples (multiplied by the calculated field enhancement factors for the MO measurements).

MAGNETO-OPTICAL MEASUREMENTS

The magneto-optical (MO) technique is described in detail in [4]. It uses the strong Faraday effect in YFe garnet to measure the vertical magnetic field component above a sample, in this case of superconducting material. The spatial resolution attained is ~ 5 -10 microns. The garnet is placed on the face of the sample to retain the highest possible sensitivity. The technique is able to resolve fields of the order of 1 mT. The sample is typically a 5×5 mm² rectangle (~ 2 mm thick). Via indirect cooling with a cold finger containing liquid helium the sample temperature was held at temperatures between 5.6-7 K. An external solenoid is used to apply a vertical magnetic field on the sample. Fig. 4 also shows the calculated vertical field distribution above a perfectly superconducting sample ($H < H_{c1}$). Strong field enhancement of up to a factor 2.7 (for a 2 mm thick sample) was calculated with a FE model for the edges of the $5 \times 5 \times 2$ mm³ sample. The field enhancement is reduced in the corners, producing the very characteristic field penetration pattern that will appear in the following figures. This enhancement factor needs to be taken into account when choosing the external field strength during a test. The MO measurements in fact showed field penetration occurring at the mid-points of the edges of the sample at external magnetic fields approximately 2.7 times smaller than the $H_{c1}(T)$ predicted on the basis of the DC magnetization measurements shown in Fig. 3. The measurement typically consists of varying the external magnetic field and measuring the field distribution on the surface of the sample by the MO indicator.

Fig. 5 shows the results of magneto-optical measurements on a sample of regular sheet material (BCP2_S_HT1_MO). The applied fields are close or above H_{c1} . Note that the field is enhanced along the edges of the sample, especially in the edge mid-points. The field exceeds H_{c1} in these areas and penetrates

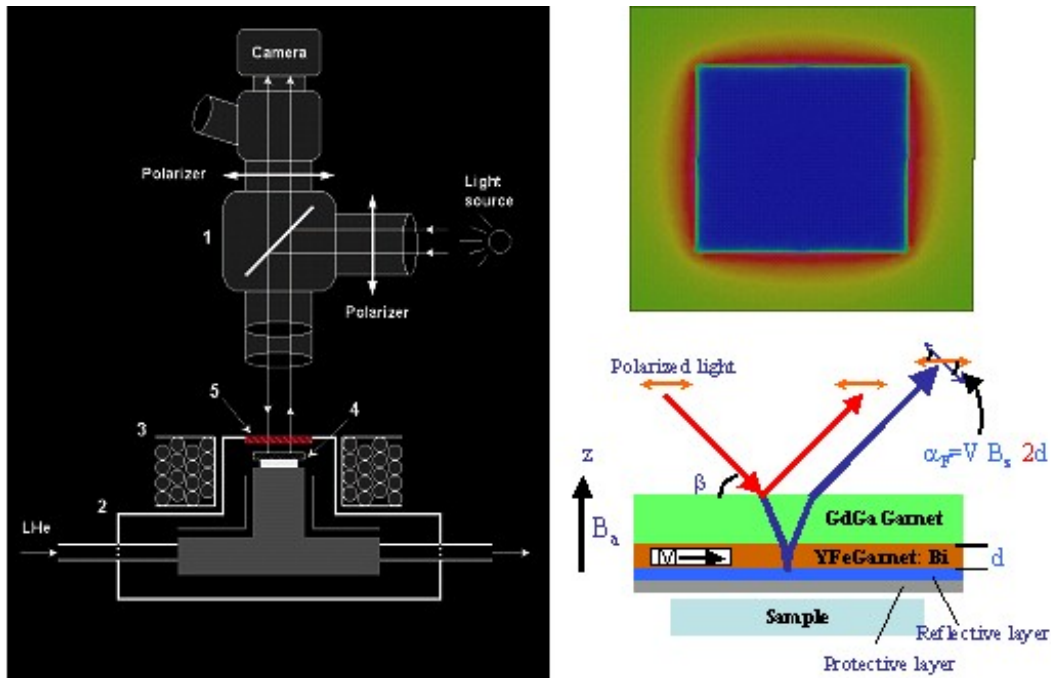


FIGURE 4. Left: MO setup at the UW ASC. Right top: calculated distribution of the vertical field on top of a superconducting sample in the Meissner state. Due to geometry related field enhancement the field is strongest in the mid-points of the four edges. Bottom right: principle of MO;

into the sample. The boundary between the dark, field-free and the light area is approximately the contour of H_{c1} . The observed behavior is as expected, with Meissner shielding in the sample preventing flux penetration, except for the areas where the critical field is exceeded. An interesting feature of the result is the irregular pattern on the fringes of the flux free regions. The characteristic spatial dimension of those features is consistent with the sample grain size, possibly hinting at the grain-boundary issues found in the large grain samples, which will be discussed next.

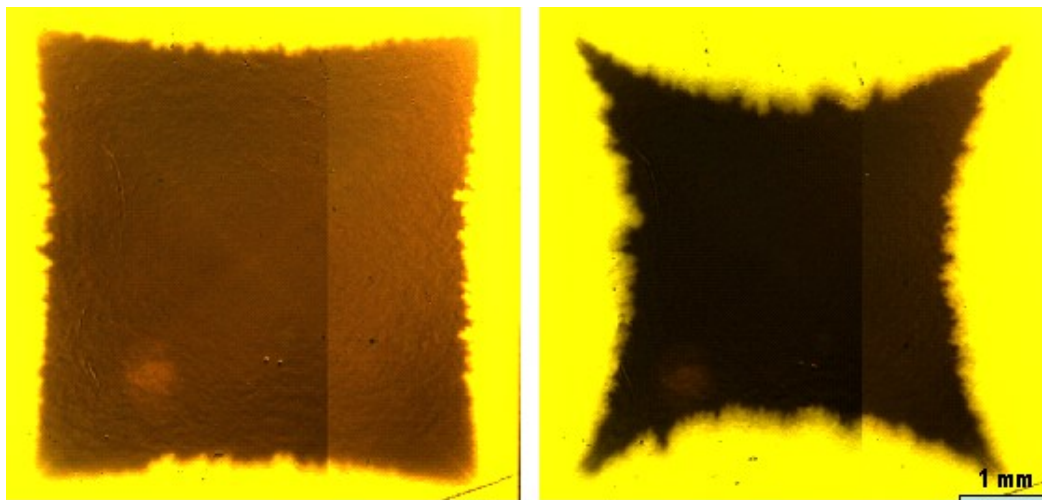


FIGURE 5. MO measurement of regular sheet material (“BCP2”) in increasing external field at 6 K Left: 60 mT, Right: 80 mT. Sample thickness 1 mm.

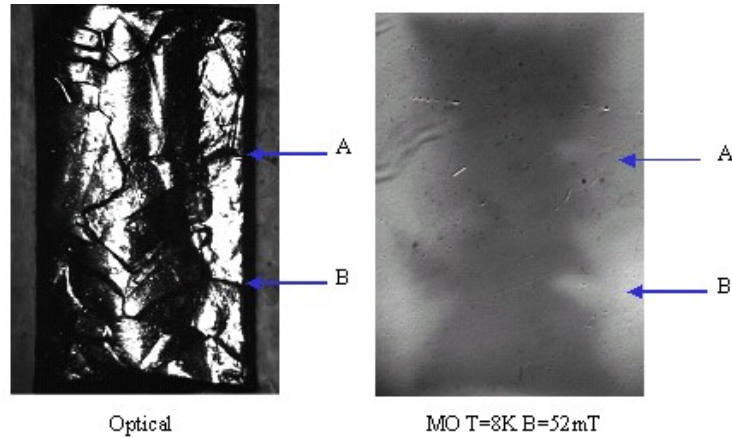


FIGURE 6. MO measurement of large grain weld sample (“BCP1”) in 52 mT external field at 8 K Left: optical image, Right: MO-image.

First measurements on a large grain weld sample (BCP1_W_HT1_RRR) showed evidence of preferential flux penetration along the grain boundaries (Fig. 6). The sample was not optimized for the MO setup. Being quite narrow (~2.5 mm) the surface was bowed as a result of the etching. The possibility of flux leakage into the sample as a result of geometry effects could not be ruled out. Therefore the experiment was repeated with a sample such as used in the test shown in Fig. 5 with the exception that the samples were heat treated at 1250°C for 24 hrs at TJNAF to grow large grains. The larger grains would make this sample similar to the weld sample. Although the high temperature heat treatment was performed in vacuum ($\sim 10^{-6}$ Torr), a degradation of the RRR by a factor of two was observed. This behavior is expected and believed to be the result of diffusion of surface oxygen into the bulk. It has to be expected that this also reduced H_{c1} in this sample. Fig. 7 shows one of the results obtained in the larger grain samples (BCP2_S_HT2_MO). The external field was 57 mT in this experiment, which is above H_{c1} at the sample temperature of 7 K, taking into account the field enhancement at the sample edges. As expected, field penetration occurs along the edges of the samples as a consequence of field enhancement, which drives the field locally above H_{c1} . What is unexpected, however, is the presence of field in the center of the sample. This field leakage occurs fast initially and then gradually increases over a time frame of several minutes. This finding corroborates the initial MO results obtained on the weld sample (Fig. 6). Most importantly, however, the flux pattern in the center of the sample reflects the grain structure. This could be an indication for suppressed or weakened

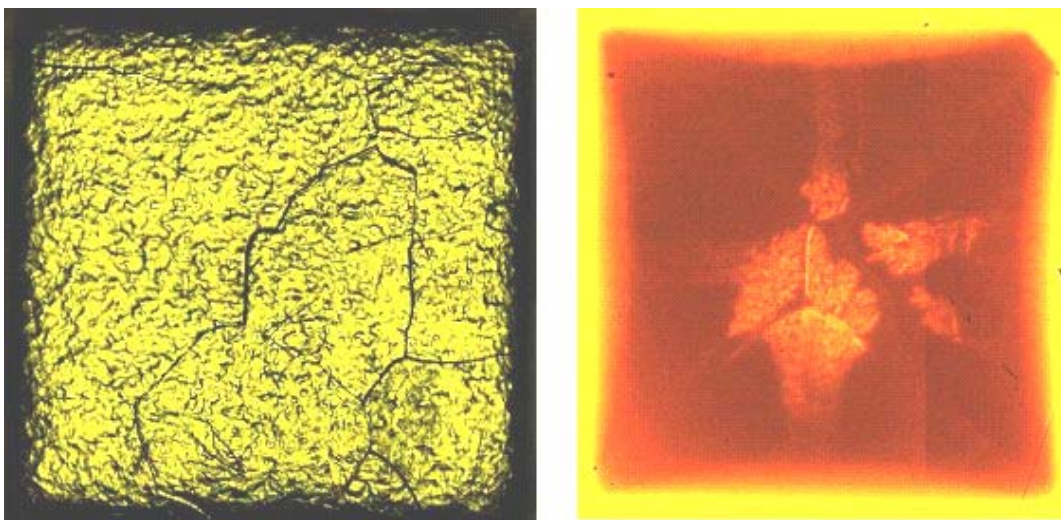


FIGURE 7. MO measurement of large grain sample in 57 mT external field at 7 K. Left: optical image, Right: MO-image. Sample thickness: 2.11 mm.

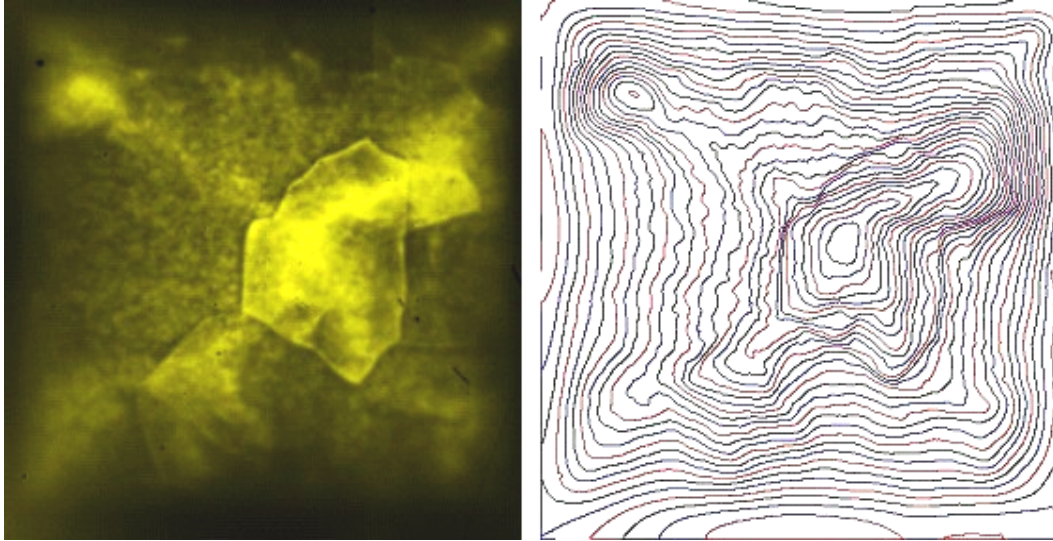


FIGURE 8. MO measurement of large grain sample in zero external field at 6 K, after returning from 120 mT. Left: MO image, Right: Current contour map. Sample thickness: 2.11 mm.

superconductivity in some grain boundaries. This could possibly be related to one of the striking features of this and the weld samples, namely that the grain-boundaries are quite deep. Fig. 8 shows the internal flux in the remanent state. In this case the external field is reduced from above H_{c2} to zero. In this condition the shielding currents trap significant field inside the superconducting sample. The right part of Fig. 8 shows a 2D current streamline inversion of the MO field map using a current sheet approximation. This is not strictly accurate for this 3D samples but will not be qualitatively wrong. The current map clearly shows that the currents cannot cross some of the grain-boundaries around the prominent central grain. This, together with the flux penetration, is possible evidence of suppressed superconductivity in the grain boundaries. Note that in Fig.8 the expected “roof-top” pattern (cross between diagonals) of the trapped flux is superimposed on the grain related features, indicating that a global shielding current flows even with the local obstructions.

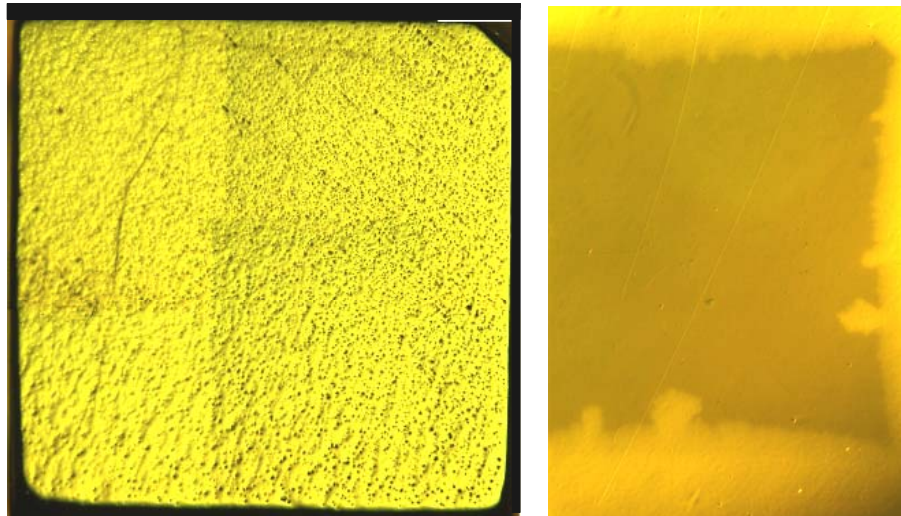


FIGURE 9. MO measurement of large grain sample after mechanical polishing in 80 mT external field at 5.6 K, Left: optical image, Right: (partial) MO-image. Sample thickness: 2.0 mm.

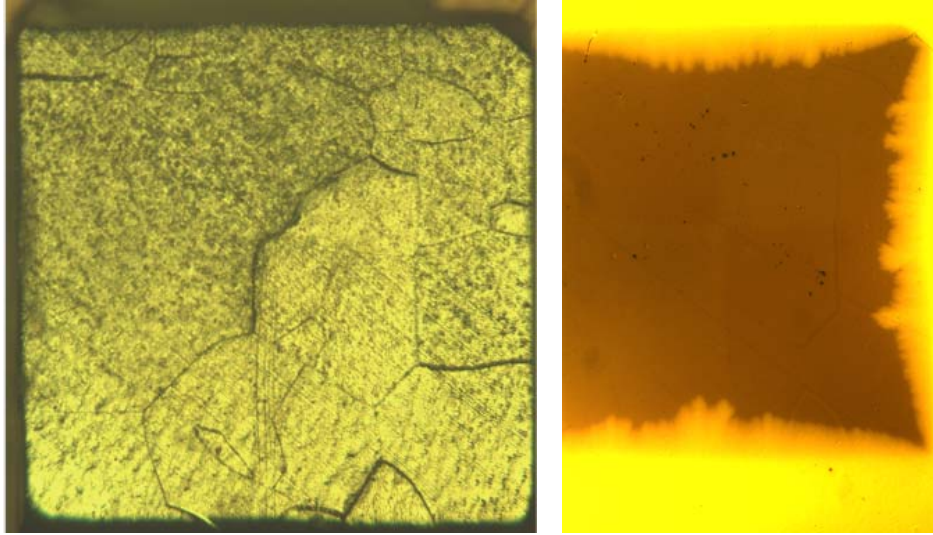


FIGURE 10. MO measurement of large grain sample after mechanical polishing and subsequent etching in 48 mT external field at 6 K, Left: optical image, Right: (partial) MO-image. Sample thickness: 2.0 mm.

Smoothing of the samples was performed by mechanical polishing techniques in order to remove topological features clearly observed in Fig. 7. After flattening the sample, the grain boundary flux penetration effect had mostly vanished. Fig. 9 shows the MO pattern in an external field well above H_{c1} (if taking into account the field enhancement). The pattern is similar to that of the “regular” sample shown in Fig. 5. Etching with a standard metallographic polishing solution (50 % H₂O, 37% HNO₃(aq), 13% HF(aq), by volume) resulted in the removal of the smeared niobium that had filled the grain boundaries and more or less reinstated the optical appearance of the surface of before polishing. Fig. 10 shows the MO pattern in an external field above H_{c1} (at the sample edges), indicating that there is no flux penetration into the center in this case. Fig. 11 shows the remanent field profile and 2D current streamlines for this case. Comparison with Fig. 8 clearly shows that a more or less perfect field-trapping pattern was found again after the polishing and etching.

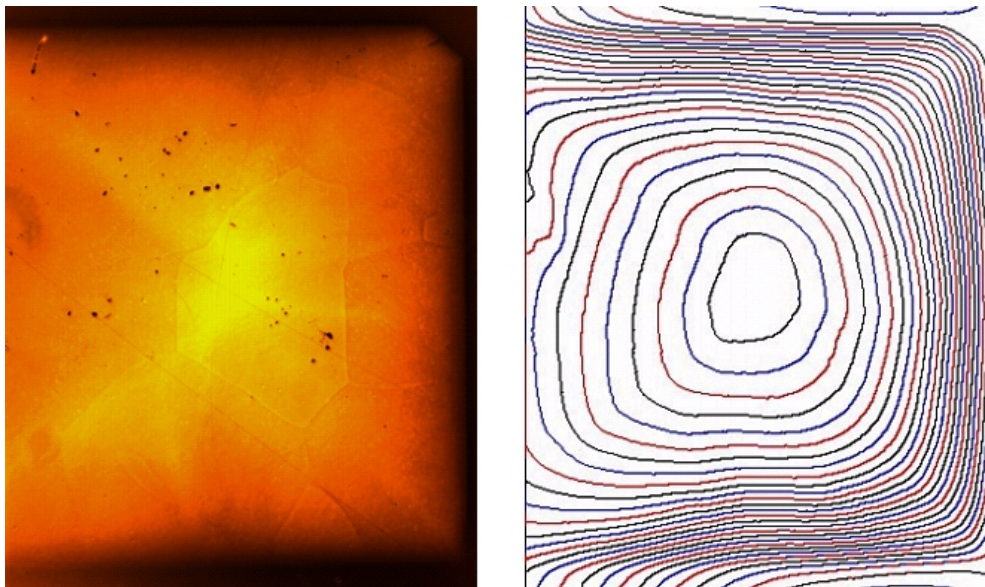


FIGURE 11. MO measurement of large grain sample after mechanical polishing etching in zero external field at 6 K, after returning from 120 mT. Left: MO image, Right: Current contour map. Sample thickness: 2 mm.

DISCUSSION

Recently Fermilab and the Applied Superconductivity Center (ASC) at the University of Wisconsin (UW) have joined forces to investigate the properties of the high purity niobium used in the cavity fabrication. Besides microscopy and chemical analysis, the focus of the material investigation is on so-called “superconducting” methods such as magnetization, specific heat and magneto-optics. Extensive SEM work was performed to characterize the surface topology. New characterization methods, such as software-based profilometry, were applied. The SEM analysis revealed deep grain boundary grooving in the weld samples. The “regular” (or fine-grain) material had the “typical” appearance of BCP etched surfaces. Following the surface characterization, magneto-optical measurements were performed, which consisted of the measurement of the magnetic field above the superconducting samples when exposed to a growing (or decreasing) external magnetic field. Two types of behavior were found. In the small grain material the expected field expulsion from the inside of the superconducting sample was observed. The magneto-optical measurements in the large grain samples showed clear evidence of flux penetration into the sample, possibly through weakened grain boundaries. This could be an indication of suppressed or weakened superconductivity in the grain-boundaries leading to a breakdown of shielding.

The following discusses possible explanations for the flux penetration. The samples investigated had large grains, either as a result of welding or after a special high temperature heat treatment. The high field areas in the accelerating and deflecting mode cavities are in the equatorial welds. Therefore the weld sample investigated in this study is representative of the material in SRF cavities. In addition, the samples were prepared in the same way as cavities, including multiple etchings and heat treatments. The sample that exhibited premature flux penetration to the core on the other hand, was not representative of the cavity case because in a cavity the 1250°C / 24 hrs heat treatment would have been combined with Ti purification to prevent the bulk contamination of the material. In fact the RRR of this sample dropped from ~450 to 280 as a result of this high temperature heat treatment, indicating the diffusion of oxygen and other impurities from the surface into the bulk.

Fig. 12 shows two schematics representing possible avenues of explanation for the flux penetration. Scenario a) is the so-called topological scenario, which explains the presence of flux inside the sample as a result of a combination of topological effects: a lower lying “valley” that connects the prominent central grain to the corner of the sample represents a region of reduced sample thickness, with further field enhancement and increased distance between MO indicator film and sample. These topological features could allow leaking of field in between the sample and the indicator film and therefore lead to an increase of the vertical flux in the center of the sample. It is not clear at this point how important this effect is and we are further planning to perform finite element model calculations to further clarify this issue. The topological hypothesis can easily explain why the flux penetration into the sample did not occur after

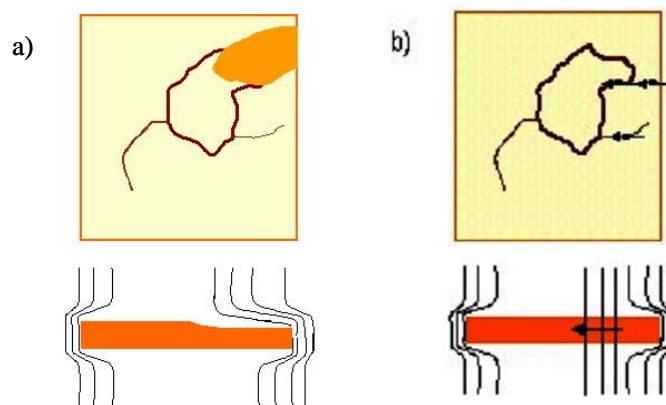


FIGURE 12. Possible scenarios to explain flux leakage into the center of the big grain sample: Left: topological, Right: weakened grain-boundaries;

polishing – this because the topological features making the flux leakage possible were removed during smoothening. The fact, however, that after the last etching step the flux penetration did not return although most of the topological features did, goes against the topological explanation.

Scenario b) assumes that flux penetrated into the center of the sample through grain boundaries with weakened superconductivity, possibly along the grain-boundaries connecting the prominent center grain to the sample edge. These grain-boundaries were found to penetrate the sample entirely from the top to the bottom face. This so-called chemical hypothesis is the preferred model for the explanation of the MO measurement results. Reduced superconductivity parameters are expected in the grain-boundaries. Flux penetration through grain boundaries is a well-known phenomenon in high temperature superconductors [5]. Strongly suppressed superconductivity in the grain boundaries of polycrystalline niobium used for SRF cavities can lead to increased surface resistance due to increased BCS resistance, hysteresis loss due to Josephson flux penetration deep into the bulk along the grain boundaries and reduced critical field. Further studies are needed to understand the exact causes of the flux penetration through the grain-boundaries.

REFERENCES

1. L. Bellantoni, N. Solyak, I. Gonin, T. Berenc, H. Edwards, M. Foley, N. Khabiboulline, D. Mitchell “Test Results of the 3.9 GHz Cavity at Fermilab”, presented at the LINAC 2004 Conference, Luebeck, Germany, Sept. 2004.
2. C. Antoine et al, “Morphological Study of Niobium Samples after Various Surface Treatments”, IX RF Superconductivity workshop, Sept. 1999, Santa Fe, USA.
3. C. Boffo, “Magnetization Measurements at 4.2K of Multifilamentary Superconducting Strands”, University of Pisa Laurea thesis, also available as Fermilab Technical Division internal memo TD-99-074, Dec. 1999.
4. A. A. Polyanskii, D. M. Feldmann, and D. C. Larbalestier, "Magneto-Optical Characterization Techniques," "The Handbook on Superconducting Materials," Edited by David Cardwell and David Ginley, Institute of Physics UK , pp. 1551, 2003.
5. D. M. Feldmann, J. L. Reeves, A. A. Polyanskii, G. Kozlowski, R. R. Biggers, R. M. Nekkanti, I. Maartense, M. Tomsic, P. Barnes, C. E. Oberly, T. L. Peterson, S. E. Babcock, and D. C. Larbalestier, “Influence of Nickel Substrate Grain Structure on YBa₂Cu₃O_{7-x} Supercurrent Connectivity in Deformation-Textured Coated Conductors”, *Appl. Phys. Lett.* 77 (18): 2906-2908 (2000).